JASA ARTICLE

Validity of the effective sound speed approximation in parabolic equation models for wind turbine noise propagation

Bill Kayser,[1,a)] David Mascarenhas,[2] Benjamin Cotté,[2] David Ecotière,[1] and Benoit Gauvreau[3]

[1]*Joint Research Unit in Environmental Acoustics, Centre for Studies on Risks, Mobility, Land Planning and the Environment, Université Gustave Eiffel, 11 rue Jean Mentelin-BP 9, 67035 Strasbourg, France*

[2]*Institut des Sciences de la Mécanique et Applications Industrielles, École Nationale Supérieure de Techniques Avancées Paris, CNRS, Commissariat a l'Energie Atomique, Electricité de France, Institut Polytechnique Paris, Paris, France*

[3]*Joint Research Unit in Environmental Acoustics, Université Gustave Eiffel, Centre for Studies on Risks, Mobility, Land Planning and the Environment, Allée des Ponts et Chaussée, Route de la Bouaye, 44340 Bouguenais, France*

ABSTRACT:

Parabolic equation (PE) based methods are widely used in outdoor acoustics because they can solve acoustic propagation problems above a mixed ground in a refractive and scattering atmosphere. However, recent research has shown phase error due to the effective sound speed approximation (ESSA). To overcome these limitations, a new PE formulation derived without the ESSA has been proposed recently. We investigate the impact of such phase error on wind turbine noise modeling, as the classical wide-angle parabolic equation (WAPE) with ESSA is widely used in the research community. We propose a comparison between the classical WAPE with ESSA and the new WAPE derived without the ESSA in the context of wind turbine noise. We highlight large phase error (several dB) on monochromatic calculations with a point source. Using an extended sound source representative of a wind turbine, we show small phase error (<1 dB) in a wind turbine noise context where sound level variability far from the source is of several dB. The validity of previous works using WAPE with ESSA is, thus, not questioned, although we do recommend the use of the new WAPE derived without the ESSA to accurately model the effect of wind speed on sound propagation. https://doi.org/10.1121/10.0017653

(Received 16 November 2022; revised 15 February 2023; accepted 6 March 2023; published online 20 March 2023)

[Editor: Michael J. White] Pages: 1846–1854

I. INTRODUCTION

Parabolic equation (PE) based methods are widely used to approximate the wave equation while modeling acoustic wave propagation in the atmosphere (e.g., Blanc-Benon *et al.*, 2001; Gauvreau *et al.*, 2002; White and Gilbert, 1989), including wind turbine noise (e.g., Barlas *et al.*, 2017; Cotté, 2018; Kayser *et al.*, 2019; Kayser *et al.*, 2022). Indeed, PE based methods can take into account the range-dependent phenomena (i.e., ground and atmospheric effects) that occur between the acoustic source and a far-field receiver, such as refraction, scattering, reflection, and absorption. This approximation is commonly used as it allows one to easily include the convection and refraction effects due to the wind. The main limitations of these methods are the small validity angle with respect to the nominal propagation direction (e.g., Lee *et al.*, 2000) and phase error due to the effective sound speed approximation (ESSA). A new formulation called extra-wide-angle PE that does not use the ESSA has been recently proposed to overcome the phase error limitation (Ostashev *et al.*, 2020). However, if phase error is an important issue when using a point source and relatively high wind speed (i.e., Mach number greater than 0.05), an underlying assumption is that phase error could be expected to be smaller when the source is very large. However, to date, there is no study that quantifies the phase error for an extended sound source like a wind turbine, while PE based methods have already been used in this context.

Thus, this paper proposes a quantitative comparison in the context of wind turbine noise between simulations done with the classical wide-angle parabolic equation (WAPE) using ESSA and simulations done with WAPE that do not use the ESSA in a moving medium to estimate if phase error induced by ESSA approximation leads to a crucial problem for modeling wind turbine noise propagation. The paper is structured as follows: Sec. II reviews the theories of the modeling, Sec. III describes the studied scenarios, Sec. IV discusses the results of the analysis, and Sec. V gives synthetic results and perspectives of this numerical study.

II. REVIEW OF THEORIES

A. WAPEs in moving and motionless atmospheres

Ostashev *et al.* (2020) have recently proposed extra-wide-angle parabolic equation (EWAPE) for sound wave propagation in a moving medium with arbitrary Mach numbers M_x. In a two-dimensional (2D) vertical plane (x, z), assuming that the air density is a constant equal to ρ_0, Eqs. (27) and (39) of Ostashev *et al.* (2020) for the sound

a)Electronic mail: bill.kayser@univ-eiffel.fr

pressure $\hat{p}(x,z)$ and for the velocity potential $\hat{\phi}(x,z)$ in the frequency domain reduce to

$$\hat{p}(x,z) = \left(1 + \frac{iM_x}{k_0}\frac{\partial}{\partial x}\right)\hat{\phi}(x,z), \tag{1}$$

$$\left(\frac{\partial}{\partial x} - ik_0\gamma_x^2\sqrt{1+\varepsilon+\hat{\mu}} + ik_0\hat{\tau}\right)\hat{\phi}(x,z) = 0, \tag{2}$$

where $k_0 = \omega/c_0$ is the wavenumber associated with the reference sound speed c_0, $\gamma_x^2 = 1/(1-M_x^2)$, $\varepsilon = (c_0/c)^2 - 1$ is the deviation of the refractive index from unity, $\hat{\mu} = (1/\gamma_x^2 k_0^2)(\partial^2/\partial z^2)$, and $\hat{\tau} = M_x\gamma_x^2\sqrt{1+\varepsilon}$. In the absence of flow, $M_x = 0$, $\gamma_x^2 = 1$, and $\hat{\tau} = 0$, and the classical PE is retrieved (Salomons, 2001),

$$\left(\frac{\partial}{\partial x} - ik_0\sqrt{1+\varepsilon+\frac{1}{k_0^2}\frac{\partial^2}{\partial z^2}}\right)\hat{p}(x,z) = 0. \tag{3}$$

From Eq. (3), the ESSA consists in considering $\varepsilon = (c_0/c_{\text{eff}})^2 - 1$, where $c_{\text{eff}} = \sqrt{\gamma R T(z)} + U(z)\cos\theta$ is the vertical effective sound speed profile that depends on the heat ratio γ, the perfect gas constant $R = 8.31\,\text{J}\cdot\text{mol}^{-1}\cdot\text{K}^{-1}$, the temperature $T(z)$ and wind speed $U(z)$ at height z above the ground, and the propagation angle θ between wind direction and source-receiver direction.

As suggested by Ostashev *et al.* (2020), the square-root operator in Eq. (3) can be approximated with a Padé (n, n) series expansion, with an angular validity that increases with n. For wind turbine noise applications, an angular validity of approximately 30° (Collins, 1993; Salomons, 2001) with respect to the horizontal direction x is generally sufficient since the receivers are typically located more than 500 m from the wind turbine; thus, a Padé (1,1) approximation can be used. Introducing the variable $\bar{\phi}$ related to the velocity potential $\hat{\phi}$ by $\hat{\phi}(x,z) = \exp(ik_0x)\bar{\phi}(x,z)$, Eq. (2) can be rewritten,

$$\Psi_1(x,z)\frac{\partial\bar{\phi}}{\partial x} = ik_0\Psi_2(x,z)\bar{\phi}, \tag{4}$$

where the functions Ψ_1 and Ψ_2 are given by

$$\Psi_m = h_{m,0} + \frac{h_{m,2}}{k_0^2}\frac{\partial^2}{\partial z^2}, \quad m = 1,2. \tag{5}$$

The coefficients $h_{m,j}$ are written as

$$h_{1,0} = 1 + b_{1,1}\varepsilon, \qquad h_{1,2} = b_{1,1}/\gamma_x^2,$$
$$h_{2,0} = a_{1,1}\gamma_x^2\varepsilon - (1+b_{1,1}\varepsilon)\tilde{\tau}, \quad h_{2,2} = a_{1,1} - b_{1,1}\tilde{\tau}/\gamma_x^2,$$

with $a_{1,1} = 1/2$, $b_{1,1} = 1/4$. The function $\tilde{\tau}$ is defined as

$$\tilde{\tau} = M_x\gamma_x^2\left(\sqrt{1+\varepsilon} - M_x\right) = \hat{\tau} - M_x^2\gamma_x^2.$$

As in the classical wide-angle PE, the Crank–Nicholson (CN) algorithm can be used to reduce Eq. (4) to a matrix system that can be easily solved. The variable $\bar{\phi}$ is discretized using a Cartesian mesh of size $\Delta x = \Delta z = \lambda/10$: $\phi_m^n = \bar{\phi}((m-1)\Delta x, (n-1)\Delta z)$, with λ the wavelength. The domain is bounded by a ground with an acoustic impedance condition at $z = 0$ and by an absorbing layer at the top of the domain. The details are given in Appendix A.

In a second step, the acoustic pressure $\hat{p}$ can be calculated from ϕ_m^n at $x_m = m\Delta x$ and $z_n = n\Delta z$ using a second-order centered finite difference scheme [Ostashev *et al.* (2020), Eq. (84)],

$$\hat{p}(x_m,z_n) = e^{ik_0x_m}\left[(1-M_x)\phi_m^n + \frac{iM_x}{2k_0\Delta x}\left[\phi_{m+1}^n - \phi_{m-1}^n\right]\right]. \tag{6}$$

The starting field is defined as (Salomons, 2001)

$$\overline{\phi}(0,z_s) = \sqrt{ik_0}\left(A_0 + A_2k_0^2z_s^2\right)e^{-k_0^2z_s^2/B}, \tag{7}$$

with $A_0 = 1.3717$, $A_2 = -0.3701$, $B = 3$, and $z_s = z - h_s$, where h_s is the source height.

B. Validation of PE against analytical solution

Following Ostashev *et al.* (2020) (pp. 3980–3982), the WAPE_M [Eq. (4)] and WAPE_ESSA [Eq. (3)] implementations are validated against an analytical solution for uniformly moving medium (constant wind vertical profile), in the presence of a perfectly flat and rigid ground. Figure 1 presents results for frequencies $f = 50$, 250, and 1000 Hz with a point source placed at $z = 80$ m (representative of the hub height of a typical wind turbine), a Mach number of $M_x = 0.05$ (typical maximum operating wind speed of a wind turbine), and a receiver height $z_r = 2$ m.

Results show that both PE methods do not predict sound pressure correctly in close range (up to 150 m), which is due to the angular validity. A good agreement between WAPE_M and the analytical solution is observed for distances above 150 m. On the other hand, the WAPE_ESSA does not predict the sound pressure correctly, with shifts in location of interference patterns. These observations are consistent with the results of Ostashev *et al.* (2020).

C. Description of the wind turbine noise model

For modern wind turbines, for which rotor diameter is very often larger than 80 m, sound pressure level (SPL) predictions are more realistic when using an extended sound source modeling. For this purpose, we use an emission model based on Amiet theory (Amiet, 1975, 1976; Roger and Moreau, 2010) that considers both trailing edge noise and turbulent inflow noise for a blade profile NACA 63415. The emission model is coupled to the PE models thanks to the *moving monopole approach* following Cotté (2019) and Kayser *et al.* (2022), which allows us to consider propagation effects between the source and the receivers to calculate wind turbine SPL in an outdoor environment. The wind

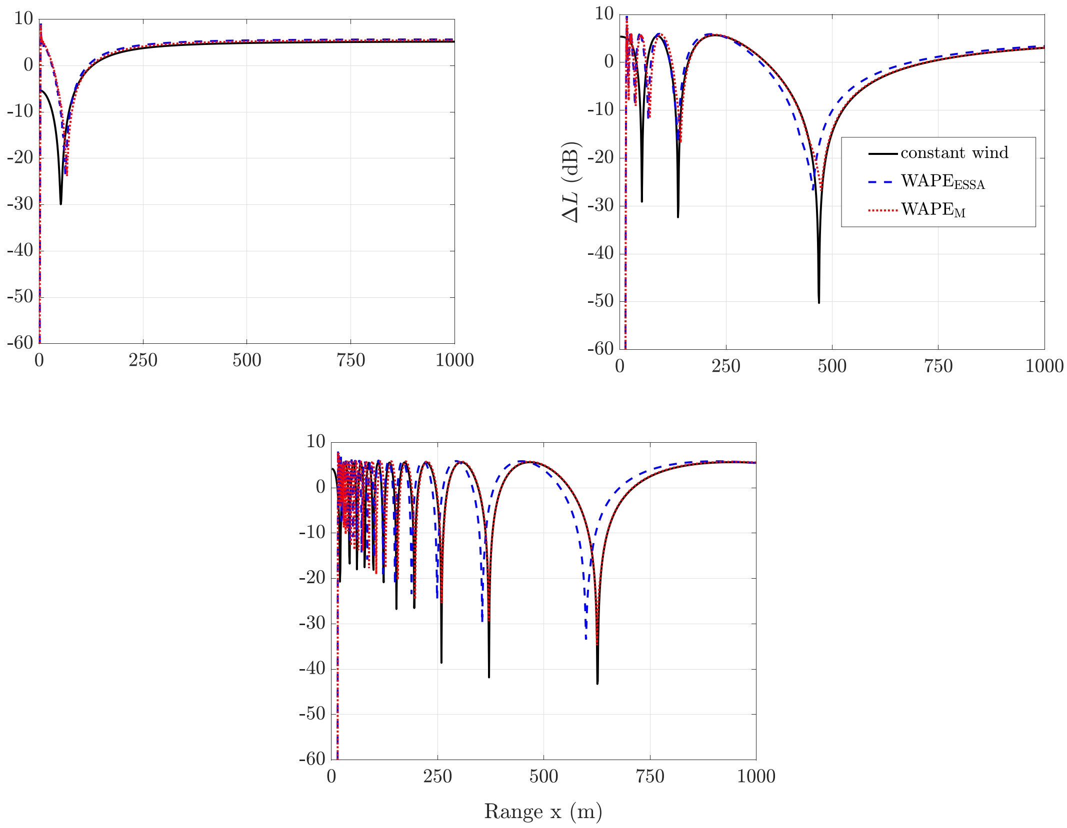

FIG. 1. (Color online) Sound pressure relative to free field ΔL for a point source at $z = 80$ m above a rigid ground in a 2D homogeneous uniformly moving medium with Mach number $M_x = 0.05$ and receiver height $z_r = 2$ m. Results are shown for analytical solution and predictions obtained with $\text{WAPE}_{\text{ESSA}}$ and WAPE_{M} for $f = 50$ Hz (top), $f = 250$ Hz (middle), and $f = 1000$ Hz (bottom).

turbine is located at $(x = 0, y = 0, z = 0)$, with its blades rotating in the (y, z) plane (see Fig. 2).

Since the incident flow is not uniform along a blade, a strip theory is used that consists in splitting each blade into D sections of variable chord c_d and span L_d, so as to fulfill the condition $L_d/c_d \geq 3, d = 1, \ldots, D$ with $D = 8$. The SPL at the receiver location $(x_r,\ 0,\ z_r)$ is calculated for a blade segment at an angular position Φ, using the point source approximation (Salomons, 2001),

$$\begin{aligned}\text{SPL}(\omega, \Phi) = &\overbrace{\text{SWL}(\omega, \Phi)}^{\text{emission}} \overbrace{-10\log\left(4\pi R_1^2\right)}^{\text{geometrical spreading}} \\ &\underbrace{+\Delta L(\omega, \Phi) - \alpha_{\text{abs}}(\omega) R_1}_{\text{atmospheric and ground effects}},\end{aligned} \tag{8}$$

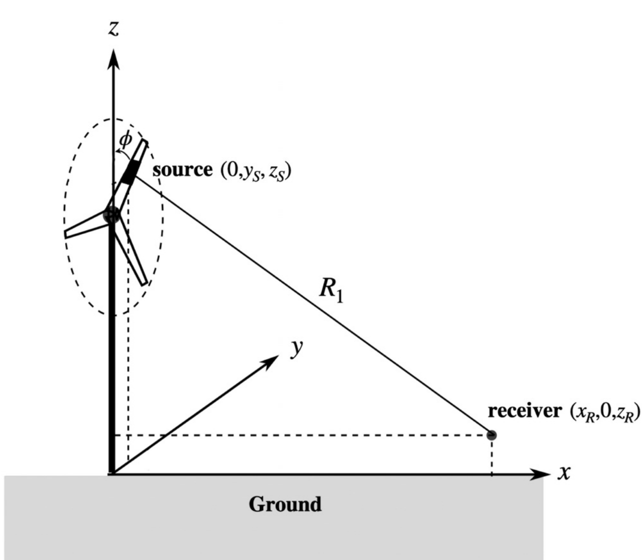

FIG. 2. Schematics of the moving monopoles approach geometry. The receiver is located at $(x_R, 0, z_R)$, and the source is located at $(0, y_s, z_s)$. R_1 is the source-receiver distance, and ϕ represents here the angular position of the blade segment.

TABLE I. Summary of the four different scenarios for the comparison of $\text{WAPE}_{\text{ESSA}}$ and WAPE_{M} predictions.

	Scenarios			
	Point source		Extended source	
Parameters	1. Reflective ground Stable atmosphere	2. Natural ground Stable atmosphere	3. Natural ground Stable atmosphere	4. Natural ground Neutral atmosphere
α wind shear exponent	0.15	0.15	0.15	0.55
σ (kN $\cdot$ s $\cdot$ m^{-4}) airflow resistivity of ground	∞	500	500	500
l_c (m) correlation length of roughness	0	0.5	0.5	0.5
σ_h (m) standard deviation of roughness heights	0	0.025	0.025	0.025

TABLE II. Number of monochromatic calculations N_f per one-third octave band of nominal frequency f_c.

f_c (Hz)	50	63	80	100	125	160	200	250	315	400	500	630	800	1000
N_f	1	1	1	1	3	3	3	3	3	3	5	5	7	7

where ω is the angular frequency of the sound at the receiver, $\mathrm{SWL}(\omega, \Phi)$ is the angle-dependent source sound power level calculated with the emission model, $R_1 = \sqrt{x_r^2 + y_s^2 + (z_s - z_r)^2}$ is the distance between the source located at $(0, y_s, z_s)$ and the receiver located at $(x_r, 0, z_r)$, ΔL is the sound attenuation relative to the free field calculated with PE methods, and α_{abs} is the sound atmospheric absorption coefficient in dB/m and calculated using ISO 9613-1:1993 (1993).

Equation (8) is used to calculate the SPL induced by each blade segment, over one rotation, at the receiver position. The summation of the sound contributions of all blade segments is then calculated at the receiver by assuming that all the contributions are uncorrelated (Tian and Cotté, 2016).

III. CASE STUDY

In the following, $\mathrm{WAPE_{ESSA}}$ and $\mathrm{WAPE_M}$ predictions are compared for four scenarios with increasing complexity that are defined in Table I. The $\mathrm{WAPE_M}$ is considered as the reference, and the error induced by the ESSA is quantified thanks to the absolute value of the deviation between $\mathrm{WAPE_{ESSA}}$ and $\mathrm{WAPE_M}$ predictions. This indicator is called the *error* and is plotted in the following figures.

Section IV A presents predictions for a unique point source placed at hub height $z = 80$ m, which is a strong assumption that is often used as a first approximation in the wind turbine noise community. Neutral atmospheric conditions are considered. Calculations in the presence of reflective ground (scenario 1) and absorbing and rough ground (scenario 2) are performed. Monochromatic results, one-third octave band results, and overall A-weighted sound pressure level (OASPL) results are presented.

Section IV B presents predictions when using an extended sound source modeling, which is more realistic for modern wind turbines. The wind turbine considered has a rotor diameter of 93 m, a hub height of 80 m, and three blades of 45 m length based on the NACA 63415 airfoil (Tian, 2016). The speed of rotation of blades increases linearly from 6 rpm at the cut-in wind speed of 4 m/s measured at the hub height to 16 rpm at the wind speed of 12 m/s. The ground properties are set to model an absorbing and rough ground. Predictions are

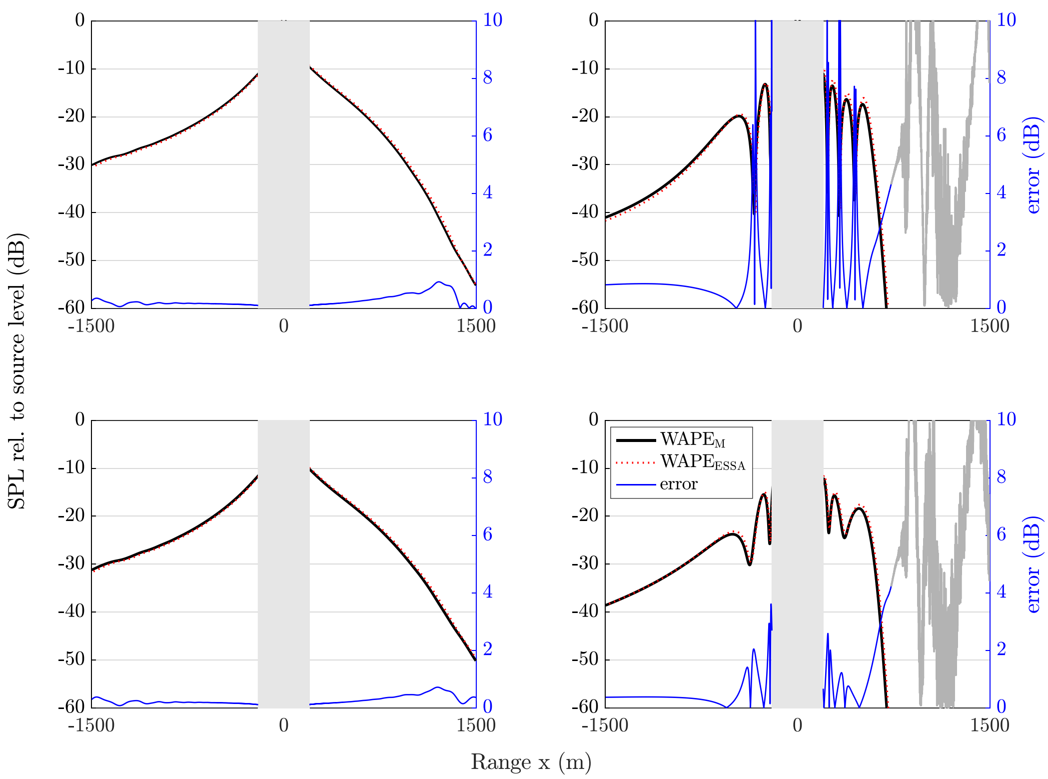

FIG. 3. (Color online) Comparison of $\mathrm{WAPE_M}$ (black line) and $\mathrm{WAPE_{ESSA}}$ (red dashed line) simulations for neutral atmospheric condition, for both flat-reflective ground (scenario 1, top) and rough-absorbing ground (scenario 2, bottom). Results are presented for the frequencies $f_c = 50$ Hz (left) and $f_c = 1000$ Hz (right), at $z_r = 2$ m. The error (blue line) between the $\mathrm{WAPE_M}$ and $\mathrm{WAPE_{ESSA}}$ simulations is plotted and depends on the right vertical axis. The error plotted in gray is associated with extremely low SPL values where numerical errors might occur as well.

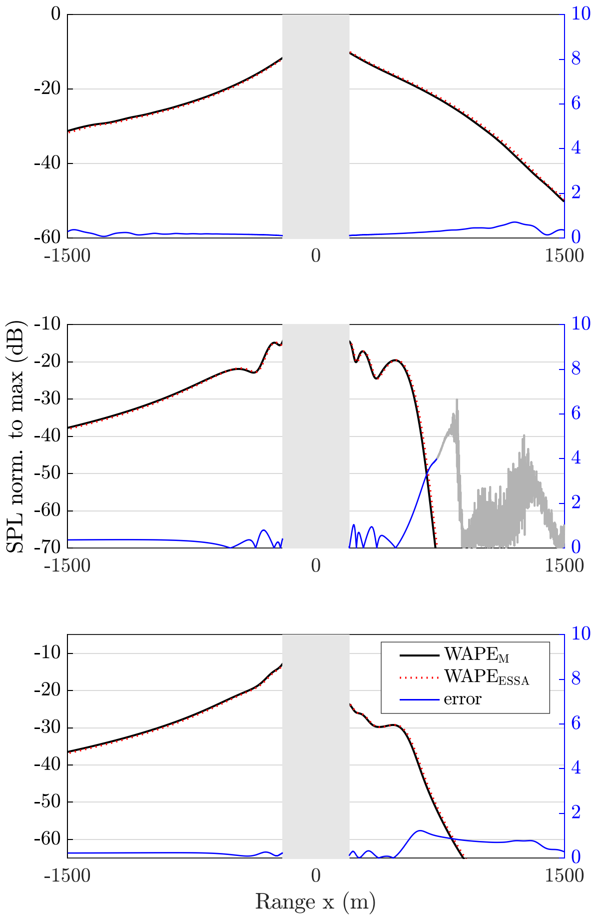

FIG. 4. (Color online) Comparison of WAPE$_M$ (black line) and WAPE$_{ESSA}$ (red dashed line) simulations for neutral atmospheric condition in the presence of rough-absorbing ground (scenario 2). Results are presented for the one-third octave band of center frequencies $f_c = 50\,\text{Hz}$ (top), $f_c = 1000\,\text{Hz}$ (middle), and OASPL (bottom), at $z_r = 2\,\text{m}$. The error (blue line) between the WAPE$_M$ and WAPE$_{ESSA}$ simulations is plotted and depends on the right vertical axis. The error plotted in gray is associated with extremely low SPL values where numerical errors might occur as well.

performed for both neutral (scenario 3) and stable (scenario 4) atmospheric conditions. Monochromatic results, one-third octave band results, and overall A-weighted SPL results are also presented.

The wind speed vertical profile $U(z)$ is defined as follows:

$$U(z) = U_{\text{ref}}\left(\frac{z}{z_{\text{ref}}}\right)^{\alpha}, \tag{9}$$

where $U_{\text{ref}} = 12$ m/s is the wind speed at hub height $z_{\text{ref}} = 80\,\text{m}$, and α is the wind shear exponent set to 0.15 for neutral atmospheric condition (scenarios 1–3) and set to 0.55 for stable atmospheric condition (scenario 4) (Van Den Berg, 2008). The wind direction is from x positive to x negative, which means that for $x \in [200; 1500]$ m, upwind conditions are considered, and for $x \in [-1500; -200]$ m, downwind conditions are considered.

For all scenarios, the atmospheric temperature is set constant at $T_0 = 10\,^{\circ}\text{C}$. As the study focuses on relatively high wind speed and given that we do not consider crosswind conditions, wind effects are considered to be predominant over temperature effects (Kayser *et al.*, 2020). Note also that phase error is mainly induced by wind effects through the effective sound speed formalism.

The ground properties (sound absorption by the ground and sound scattering by surface roughness) are taken into account through the effective admittance model (Bass and Fuks, 1979) implemented in PE methods following Kayser *et al.* (2019). The effective admittance β_{eff} is defined as

$$\beta_{\text{eff}} = \frac{1}{Z} + \beta_{\text{rough}}, \tag{10}$$

where Z is the acoustic impedance of the ground, and β_{rough} is the average effect of surface roughness on ground acoustic admittance. The impedance Z is calculated using Miki's impedance model (Miki, 1990), for which frequency validity is verified (Kirby, 2014), and that depends only on the airflow resistivity of the ground σ (kN·s·m^{-4}). The expression for β_{rough} corresponds to a 2D rough surface with a small and slowly varying roughness (Brelet and Bourlier, 2008), which depends on two parameters, l_c (m) and σ_h (m), which are, respectively, the correlation length of the horizontal variations of the ground and the standard deviation of the ground roughness heights (see Kayser *et al.*, 2022; Kayser *et al.*, 2019). In the first scenario, the ground is perfectly flat and rigid, which means that $\sigma = \infty$ kN·s·m^{-4}, $l_c = 0\,\text{m}$, and $\sigma_h = 0$ m. For scenarios 2–4, $\sigma = 500\,\text{kN·s·m}^{-4}$, which accounts for slight absorbing ground (e.g., cultivated ground), with $l_c = 0.5$ m and $\sigma_h = 0.025$ m for the corresponding ground roughness parameters (Borgeaud and Bellini, 1998; Embleton *et al.*, 1983).

Given that the one-third octave band widths increase with frequency and that the wavelengths decrease with frequency, the one-third octave band levels have to be calculated with an increasing number of monochromatic calculations with frequency (IEC 61260–1:2014, 2014) (see Table II).

The OASPL indicator is calculated for $f \in [50; 1000]$ Hz. The OASPL indicator is used with the extended sound source only and corresponds to overall A-weighted SPL, which is averaged over one blade rotation.

IV. RESULTS

A. Point source approximation

Figure 3 presents results of the comparison for scenarios 1 and 2, at the frequencies $f_c = 50\,\text{Hz}$ and $f_c = 1000\,\text{Hz}$. The comparison shows a shift in interference patterns between WAPE$_M$ and WAPE$_{ESSA}$ simulations, due to the WAPE$_{ESSA}$ phase error. The shift leads to a non-negligible error, especially at high frequencies at the position of the interference dips, i.e., up to 15 dB for flat and reflective ground and up to 4 dB for absorbing and rough ground. In downwind conditions ($x \in [-1500; 0]$ m) and outside the interference dips, only small error appears (less than 0.7 dB), whatever the frequency and ground properties. In upwind conditions ($x \in [0; 1500]$ m), the error increases up to 20 dB in the shadow zone. However, the magnitude of the error is not critical in such a region from a practical point of

https://doi.org/10.1121/10.0017653

view. Indeed, it is associated with very low SPL, as we do not consider sound scattering by turbulence and also given that other environmental sound sources are very likely to mask wind turbine sound contribution. Given the extremely low SPL in this region, the error is plotted in gray as numerical errors might occur as well. One can also notice that the shadow zone boundary is slightly moved for $f_c = 50$ Hz between the two types of ground. This observation might be explained by creeping wave (Don and Cramond, 1986). In the case study of scenarios 1 and 2, we conclude that the phase error leads to non-negligible SPL error, even in the presence of an absorbing and rough ground.

Figure 4 presents results of the comparison for scenario 2, at the one-third octave bands of center frequencies $f_c = 50$ Hz and $f_c = 1000$ Hz, as well as for OASPL. Results of Fig. 4 show low error (<0.5 dB) outside the shadow zone for the three indicators. These low errors are due to the smoothing done by using one-third octave and OASPL indicators. In the shadow zone, the magnitude of the error is still high (up to 7 dB) for one-third octave bands, but it is acceptable (<1 dBA) for OASPL.

B. Extended wind turbine source

Figure 5 shows results of the comparison for scenarios 3 and 4, at the frequencies $f_c = 50$ Hz and $f_c = 1000$ Hz for one blade rotation. Figure 5 does not show interference patterns given that the source is extended spatially and that SPLs are averaged over one blade rotation. Therefore, only small SPL error (<0.5 dB) due to phase error is observed outside the shadow zone, as the significant error is mainly due to shifts in the location of interference patterns. It should be noted that the slightly higher error that appears in downwind conditions far from the source (i.e., for $x < -1000$ m) is due to refraction effects. This is presented in more detail in Appendix B.

As in Sec. IV A, we clearly see that the error is non-negligible (up to 8 dB) in the shadow zone. As already discussed, this error is not crucial as the SPLs are very low in such region and, thus, will most likely be masked by other environmental sources or sound scattered by atmospheric turbulence (that is not taken into account here). Finally, the phase error seems slightly higher for stable atmospheric conditions. This is because the shear factor α is higher in these conditions, which induces a stronger wind vertical gradient and, thus, stronger refraction effect. Under these conditions, the ESSA limitation is more noticeable.

Figure 6 presents results for one-third octave bands of center frequency $f_c = 50$, and $f_c = 1000$ Hz as well as OASPL. The atmospheric condition is stable with $\alpha = 0.55$ as it induces the highest SPL error due to phase error (see Fig. 5). Results for one-third octave bands and OASPL show that the error curves are very similar to the monochromatic calculations (Fig. 5), with values of the same order of magnitude (<0.5 dB outside the shadow zone and caustic region). There are no major differences between the two scenarios.

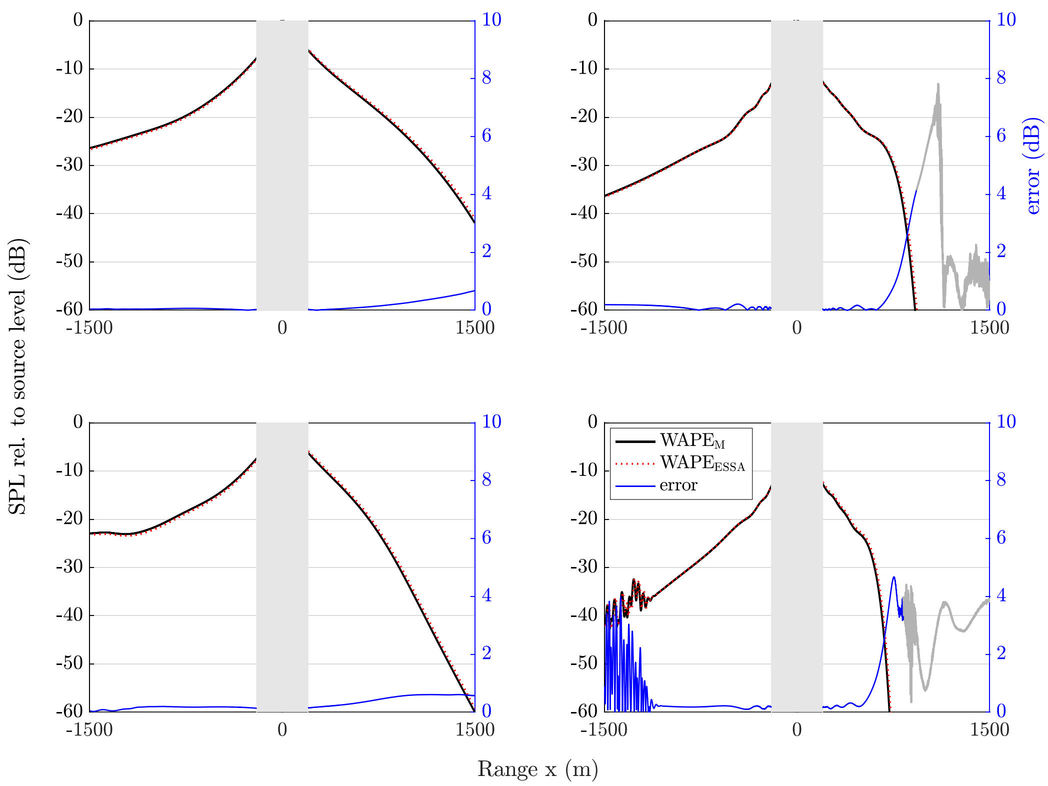

FIG. 5. (Color online) Comparison of WAPE$_M$ (black line) and WAPE$_{ESSA}$ (red dashed line) simulations with an extended sound source, for both stable (scenario 3, top) and neutral atmospheric condition (scenario 4, bottom). Results are presented for the frequencies $f_c = 50$ Hz (left) and $f_c = 1000$ Hz (right), at $z_r = 2$ m. The error (blue line) between the WAPE$_M$ and WAPE$_{ESSA}$ simulations is plotted and depends on the right vertical axis. The error plotted in gray is associated with extremely low SPL values where numerical errors might occur as well.

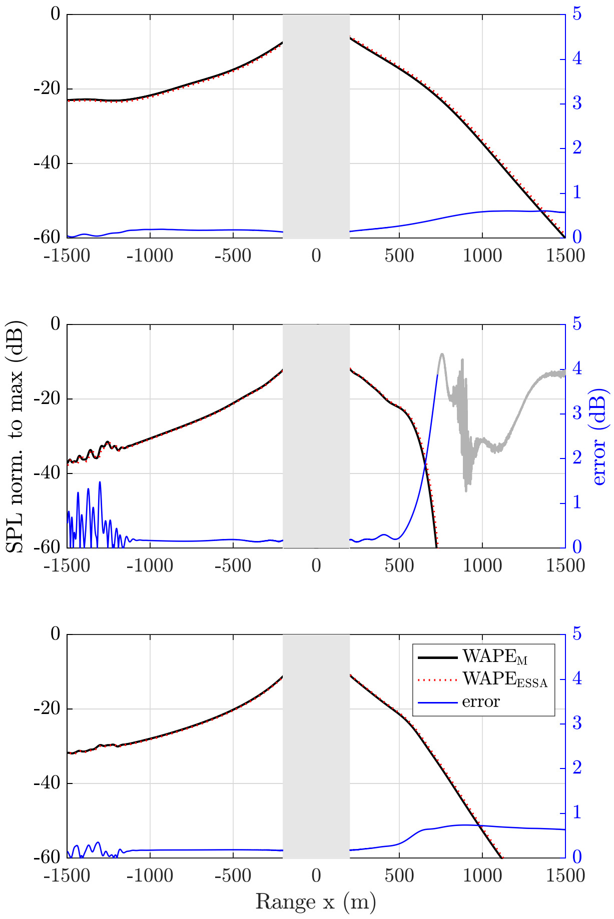

FIG. 6. (Color online) Comparison of WAPE$_M$ (black line) and WAPE$_{ESSA}$ (red dashed line) simulations with an extended sound source, for stable atmospheric condition (scenario 3). Results are presented for the one-third octave band of center frequencies $f_c = 50$ Hz (top), $f_c = 1000$ Hz (middle), and OASPL (bottom), at $z_r = 2$ m. The error (blue line) between the WAPE$_M$ and WAPE$_{ESSA}$ simulations is plotted and depends on the right vertical axis. The error plotted in gray is associated with extremely low SPL values where numerical errors might occur as well.

V. CONCLUSION AND DISCUSSION

This work focuses on SPL discrepancy predictions due to phase error induced by ESSA in the PE model, in the context of wind turbine noise. To estimate the error, comparisons are made between simulations from the WAPE model with the ESSA and the WAPE model derived without this approximation.

First, comparisons are made with a point source located at the hub height of the wind turbine, with a heterogeneous atmosphere and for both a flat-reflective ground and a rough-absorbing ground. Results highlight high phase error (up to 15 dB for flat and reflective ground) outside the shadow zone, due to shifts in interference patterns between the two WAPE model predictions. Phase error is even higher in the shadow zone (up to 20 dB for reflective ground). However, high phase error in such a region is not crucial as SPLs are very low. Thus, environmental sources are very likely to mask the wind turbine noise. A study is also performed for one-third octave band and OASPL. The results show fewer interference patterns due to smoothing by considering one-third octave bands, which leads to lower phase error ($\approx$1 dB outside the shadow zone) than for the monochromatic study.

Another comparison is performed with an extended source representative of a wind turbine, for both neutral and stable atmospheric conditions. As the wind turbine sound source is extended spatially, and the SPLs are averaged over one blade rotation, the interference patterns are significantly reduced. As a result, phase error outside the shadow zone is smaller ($<$0.5 dB) and seems negligible for this scenario. Stable atmospheric conditions show a slight increase in phase error as the wind vertical gradient is stronger and ESSA more penalizing. Furthermore, with the extended wind turbine sound source, we showed that phase error leads to negligible error on the prediction of one-third octave bands or OASPL.

In summary, we can conclude that when using a point source, the phase error induced by the ESSA can be an important issue that leads to strong error in SPL predictions, especially in the presence of interference patterns, strong refraction, and a flat and reflective ground. We conclude here that the ESSA approach should not be used if a simplified modeling of the wind turbine by a unique point source is considered. Nevertheless, when considering an extended source and more realistic scenarios (i.e., wind turbine on a rough-absorbing ground), we found that phase error due to the ESSA induced small or even negligible SPL prediction error. For this specific case study, both types of WAPE modeling produce equivalent results. Those results confirm that, even if the new WAPE formulation remains undeniably the most accurate, the WAPE formulation using ESSA can still be used for predicting wind turbine noise on the condition that the source modeling explicitly takes into account the large size of the source.

ACKNOWLEDGMENTS

This research is funded by the French National Agency for Research in the framework of the PIBE project (Contract No. ANR-18-CE04-0011). This project has also received funding from the European Union's Horizon 2020 research and innovation program under the Marie Sklodowska-Curie Grant Agreement No. 812719.

APPENDIX A: NUMERICAL SOLUTION OF THE WAPE IN MOVING MEDIUM

To solve Eq. (4), the CN scheme is used to advance the solution from x to $x + \Delta x$,

$$\left[\Psi_1 - \frac{ik_0 \Delta x}{2}\Psi_2\right]\bar{\phi}(x+\Delta x) = \left[\Psi_1 + \frac{ik_0 \Delta x}{2}\Psi_2\right]\bar{\phi}(x), \quad \text{(A1)}$$

where the terms Ψ_1 and Ψ_2 can be written

$$\Psi_1 = 1 + \frac{\varepsilon}{4} + \frac{1}{4k_0^2\gamma_x^2}\frac{\partial^2}{\partial z^2}, \quad \text{(A2)}$$

$$\Psi_2 = \frac{\gamma_x^2\varepsilon}{2} - \left(1+\frac{\varepsilon}{4}\right)\tilde{\tau} + \frac{(2\gamma_x^2-\tilde{\tau})}{4k_0^2\gamma_x^2}\frac{\partial^2}{\partial z^2}. \quad (A3)$$

The domain is now discretized with mesh sizes Δx and Δz: $\phi_m^n = \bar{\phi}((m-1)\Delta x, (n-1)\Delta z)$, with $m = 1, \ldots, M$ and $n = 1, \ldots, N$. The second derivative with respect to z is estimated using a second-order finite difference scheme,

$$\left(\frac{\partial^2}{\partial z^2}\right)\phi_m^n = \frac{\phi_m^{n+1} - 2\phi_m^n + \phi_m^{n-1}}{k_0^2\Delta z^2}. \quad (A4)$$

The numerical scheme associated with the CN for the WAPE method is, thus,

$$M_1\phi_{m+1}^n = M_2\phi_m^n, \quad (A5)$$

where the matrices M_1 and M_2 are given by

$$\begin{aligned} M_1\phi_m^n = &\left[1+\frac{\varepsilon_m^n}{4} - \frac{ik_0\Delta x}{2}\left(\frac{(\gamma_x^2)_m^n\varepsilon_m^n}{2} - \left(1+\frac{\varepsilon_m^n}{4}\right)\tilde{\tau}_m^n\right)\right]\phi_m^n \\ &+ \left[\frac{2-ik_0\Delta x(2(\gamma_x^2)_m^n - \tilde{\tau}_m^n)}{8k_0^2(\gamma_x^2)_m^n}\right]\frac{\phi_m^{n+1} - 2\phi_m^n + \phi_m^{n-1}}{\Delta z^2}, \end{aligned} \quad (A6)$$

$$\begin{aligned} M_2\phi_m^n = &\left[1+\frac{\varepsilon_m^n}{4} - \frac{ik_0\Delta x}{2}\left(\frac{(\gamma_x^2)_m^n\varepsilon_m^n}{2} - \left(1+\frac{\varepsilon_m^n}{4}\right)\tilde{\tau}_m^n\right)\right. \\ &\left. - \frac{2-ik_0\Delta x(2(\gamma_x^2)_m^n - \tilde{\tau}_m^n)}{4k_0^2(\gamma_x^2)_m^n\Delta z^2}\right]\phi_m^n \\ &+ \left[\frac{2-ik_0\Delta x(2(\gamma_x^2)_m^n - \tilde{\tau}_m^n)}{8k_0^2(\gamma_x^2)_m^n\Delta z^2}\right]\left(\phi_m^{n+1} + \phi_m^{n-1}\right). \end{aligned} \quad (A7)$$

The matrix M_1 in Eq. (A6) is tridiagonal with diagonal elements

$$\begin{aligned} b_n = &\left[1+\frac{\varepsilon}{4} - \frac{ik_0\Delta x}{2}\left(\frac{\gamma_x^2\varepsilon}{2} - \left(1+\frac{\varepsilon}{4}\right)\tilde{\tau}\right)\right. \\ &\left. - \frac{2-ik_0\Delta x(2\gamma_x^2 - \tilde{\tau})}{4k_0^2\gamma_x^2\Delta z^2}\right] \end{aligned} \quad (A8)$$

and off diagonal elements

$$a_n = c_n = \left[\frac{2-ik_0\Delta x(2\gamma_x^2 - \tilde{\tau})}{8k_0^2\gamma_x^2\Delta z^2}\right]. \quad (A9)$$

Similarly, the matrix M_2 in Eq. (A7) is tridiagonal with diagonal elements

$$\begin{aligned} e_n = &\left[1+\frac{\varepsilon}{4} + \frac{ik_0\Delta x}{2}\left(\frac{\gamma_x^2\varepsilon}{2} - \left(1+\frac{\varepsilon}{4}\right)\tilde{\tau}\right)\right. \\ &\left. - \frac{2+ik_0\Delta x(2\gamma_x^2 - \tilde{\tau})}{4k_0^2\gamma_x^2\Delta z^2}\right] \end{aligned} \quad (A10)$$

and off diagonal elements

$$d_n = f_n = \left[\frac{2+ik_0\Delta x(2\gamma_x^2 - \tilde{\tau})}{8k_0^2\gamma_x^2\Delta z^2}\right]. \quad (A11)$$

The boundary condition at $z = 0$ $(n = 1)$ written with respect to the normalized admittance $\beta = 1/Z$ can be obtained by using the centered second-order scheme at the fictitious point $z = -\Delta z$,

$$\frac{\phi_m^2 - \phi_m^0}{2\Delta z} + ik_0\beta\phi_m^1 = 0. \quad (A12)$$

The first lines of the matrices M_1 and M_2 are changed accordingly, with modified coefficients,

$$c_{1g} = 2c_1, \quad b_{1_g} = b_1 + 2ik_0\Delta z\beta c_1,$$
$$f_{1g} = 2f_1, \quad e_{1_g} = e_1 + 2ik_0\Delta z\beta f_1.$$

APPENDIX B: DOWNWIND ERRORS DUE TO REFRACTIVE EFFECT FAR FROM THE SOURCE

Figure 7 shows the presence of caustics at long distances from the source for downwind conditions, with high associated sound pressure levels. For example, with a stable

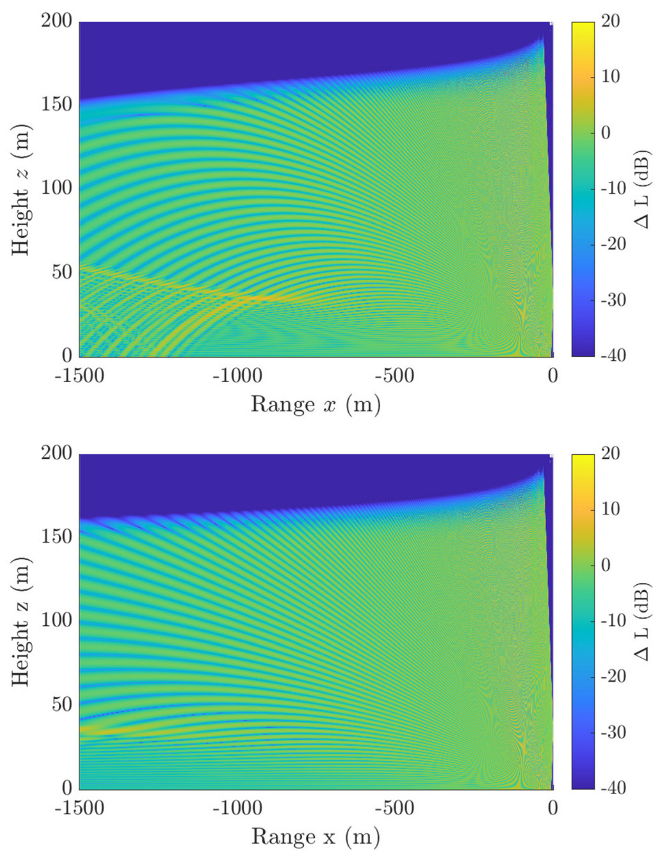

FIG. 7. (Color online) Color maps (x, z) of attenuation to free field ΔL term of Eq. (8) for downwind conditions for both stable (top) and neutral (bottom) atmospheric conditions. The source frequency is $f = 1000$ Hz, the source height is $z_s = 35$ m, and the ground is rough and absorbing. Simulations are performed with WAPE$_\mathrm{M}$ modeling.

https://doi.org/10.1121/10.0017653

atmosphere, these caustics cover a wide spatial region between heights of $z = 0$ m and $z = 60$ m. These caustics are visible in Figs. 4–6.

Amiet, R. K. (**1975**). "Acoustic radiation from an airfoil in a turbulent stream," J. Sound Vib. **41**(4), 407–420.

Amiet, R. K. (**1976**). "Noise due to turbulent flow past a trailing edge," J. Sound Vib. **47**(3), 387–393.

Barlas, E., Zhu, W. J., Shen, W. Z., Dag, K. O., and Moriarty, P. (**2017**). "Consistent modelling of wind turbine noise propagation from source to receiver," J. Acoust. Soc. Am. **142**(5), 3297–3310.

Bass, F. G., and Fuks, I. M. (**1979**). *Wave Scattering from Statistically Rough Surfaces* (Pergamon, Oxford, UK).

Blanc-Benon, P., Dallois, L., and Juvé, D. (**2001**). "Long range sound propagation in a turbulent atmosphere within the parabolic approximation," Acta Acust. united Acust. **87**(6), 659–669.

Borgeaud, M., and Bellini, A. (**1998**). "A database for electromagnetic scattering studies of bare soil surfaces," in *IGARSS '98. Sensing and Managing the Environment. 1998 IEEE International Geoscience and Remote Sensing. Symposium Proceedings (Cat. No. 98CH36174)*, July 6–10, Seattle, WA, Vol. 3, pp. 1197–1199.

Brelet, Y., and Bourlier, C. (**2008**). "Bistatic scattering from a sea-like one-dimensional rough surface with the perturbation theory in HF-VHF band," in *IGARSS 2008—2008 IEEE International Geoscience and Remote Sensing Symposium*, July 7–11, Boston, MA, Vol. 4, pp. 1137–1140.

Collins, M. D. (**1993**). "A split-step Padé solution for the parabolic equation method," J. Acoust. Soc. Am. **93**(4), 1736–1742.

Cotté, B. (**2018**). "Coupling of an aeroacoustic model and a parabolic equation code for long range wind turbine noise propagation," J. Sound Vib. **422**, 343–357.

Cotté, B. (**2019**). "Extended source models for wind turbine noise propagation," J. Acoust. Soc. Am. **145**(3), 1363–1371.

Don, C., and Cramond, A. (**1986**). "Creeping wave analysis of impulse propagation through a shadow boundary," J. Acoust. Soc. Am. **80**(1), 302–305.

Embleton, T. F. W., Piercy, J. E., and Daigle, G. A. (**1983**). "Effective flow resistivity of ground surfaces determined by acoustical measurements," J. Acoust. Soc. Am. **74**(4), 1239–1244.

Gauvreau, B., Bérengier, M., Blanc-Benon, P., and Depollier, C. (**2002**). "Traffic noise prediction with the parabolic equation method: Validation of a split-step Padé approach in complex environments," J. Acoust. Soc. Am. **112**(6), 2680–2687.

IEC 61260-1:2014 (**2014**). "Electroacoustics—Octave-band and fractional-octave-band filters—Part 1: Specifications" (International Electrotechnical Commission, Geneva, Switzerland).

ISO 9613-1:1993 (**1993**). "Acoustics—Sound attenuation in free field—Part 1: Atmospheric absorption calculation" (International Organization for Standardization, Geneva, Switzerland).

Kayser, B., Cotté, B., Ecotière, D., and Gauvreau, B. (**2020**). "Environmental parameters sensitivity analysis for the modeling of wind turbine noise in downwind conditions," J. Acoust. Soc. Am. **148**(6), 3623–3632.

Kayser, B., Gauvreau, B., and Ecotière, D. (**2019**). "Sensitivity analysis of influential parameters for wind turbine noise," in *Proceedings of the 8th International Meeting on Wind Turbine Noise Conference*, June 12–14, Lisbon, Portugal.

Kayser, B., Gauvreau, B., Écotière, D., and Mallet, V. (**2022**). "Wind turbine noise uncertainty quantification for downwind conditions using metamodeling," J. Acoust. Soc. Am. **151**(1), 390–401.

Kirby, R. (**2014**). "On the modification of Delany and Bazley fomulae," Appl. Acoust. **86**, 47–49.

Lee, D., Pierce, A. D., and Shang, E.-C. (**2000**). "Parabolic equation development in the twentieth century," J. Comput. Acoust. **8**(4), 527–637.

Miki, Y. (**1990**). "Acoustical properties of porous materials—Modifications of Delany–Bazley models," J. Acoust. Soc. Jpn. E **11**(1), 19–24.

Ostashev, V. E., Wilson, D. K., and Muhlestein, M. B. (**2020**). "Wave and extra-wide-angle parabolic equations for sound propagation in a moving atmosphere," J. Acoust. Soc. Am. **147**(6), 3969–3984.

Roger, M., and Moreau, S. (**2010**). "Extensions and limitations of analytical airfoil broadband noise models," Int. J. Aeroacoust. **9**(3), 273–305.

Salomons, E. M. (**2001**). *Computational Atmospheric Acoustics* (Kluwer Academic, Netherlands).

Tian, Y. (**2016**). "Modeling of wind turbine noise sources and propagation in the atmosphere," Ph.D. thesis, Université Paris-Saclay, Gif-sur-Yvette, France.

Tian, Y., and Cotté, B. (**2016**). "Wind turbine noise modeling based on Amiet's theory: Effects of wind shear and atmospheric turbulence," Acta Acust. united Acust. **102**(4), 626–639.

Van Den Berg, F. (**2008**). "Criteria for wind farm noise: Lmax and Lden," in *Proceedings of the Seventh European Conference on Noise control, EURONOISE, Acoustics'*08, Paris, France.

White, M. J., and Gilbert, K. E. (**1989**). "Application of the parabolic equation to the outdoor propagation of sound," Appl. Acoust. **27**(3), 227–238.